

Origin of Bursting through Homoclinic Spike Adding in a Neuron Model

Paul Channell,¹ Gennady Cymbalyuk,² and Andrey Shilnikov^{1,*}

¹Department of Mathematics and Statistics, Georgia State University, Atlanta, Georgia 30303, USA

²Department of Physics and Astronomy, Georgia State University, Atlanta, Georgia 30303, USA

(Received 20 November 2006; published 30 March 2007)

The origin of spike adding in bursting activity is studied in a reduced model of the leech heart interneuron. We show that, as the activation kinetics of the slow potassium current are shifted towards depolarized membrane potential values, the bursting phase accommodates incrementally more spikes into the train. This phenomenon is attested to be caused by the homoclinic bifurcations of a saddle periodic orbit setting the threshold between the tonic spiking and quiescent phases of the bursting. The fundamentals of the mechanism are revealed through the analysis of a family of the *onto* Poincaré return mappings.

DOI: 10.1103/PhysRevLett.98.134101

PACS numbers: 05.45.Gg, 05.45.Ac, 87.19.La

Bursting is a manifestation of complex, multiple time scale dynamics observed in various fields of science as diverse as neuroscience, food chain echo systems, and nonlinear optics [1]. Period adding, called spike adding in the context of neuronal bursting, is a generic term describing nonlinear phenomena observed also in distinct applications, such as the van der Pol generator, bubble formation, and piecewise linear endomorphisms, although the underlying mechanisms are quite dissimilar [2,3]. Studies of the bursting require nonlocal bifurcation analysis, which is based on the methods of Poincaré return mappings. The Poincaré mappings have been employed intensively in computational neuroscience [4], although a disadvantage of the commonly used pointwise ones generated from time series is that they are sparse. In this Letter, we propose a new algorithm for constructing a full family of *onto* mappings. Unlike a pointwise one, an *onto* mapping allows us to determine unstable solutions that are the primary organizing centers of complex dynamics of a system.

The spike adding cascade analyzed in this Letter acts as follows: As the bifurcation parameter shifts the half-inactivation potential towards more depolarized values, the number of spikes per burst grows incrementally with no bound until bursting transforms into tonic spiking (Fig. 1). Earlier, in Refs. [5–7] we discovered and analyzed two novel mechanisms of transitions between tonic spiking and bursting. Both describe the *terminal phases* of the spike adding cascades. The mechanisms differ by distinct homoclinic bifurcations of a saddle-node periodic orbit. So, the first one is due to the blue sky catastrophe [8], where new spikes emerge in a middle part of a burst. The second one is characterized by the bistability of the coexistent tonic spiking and bursting attractors separated by a threshold, which is the stable manifold of a saddle periodic orbit. In this case, bursting gains new spikes at its very beginning while approaching this threshold.

We study the spike adding cascade in the reduced oscillatory heart interneuron model [5,6,9]:

$$\begin{aligned}\dot{V} &= -2[30m_{K2}^2(V + 0.07) + 8(V + 0.046) \\ &\quad + 200f^3(-150, 0.0305, V)h_{Na}(V - 0.045)], \\ \dot{h}_{Na} &= 24.69[f(500, 0.0333, V) - h_{Na}], \\ \dot{m}_{K2} &= 4[f(-83, 0.018 + V_{K2}^{shift}, V) - m_{K2}],\end{aligned}\quad (1)$$

where V is the membrane potential, h_{Na} is inactivation of the fast sodium current, and m_{K2} is activation of the persistent potassium one I_{K2} ; a Boltzmann function $f(a, b, V) = 1/(1 + e^{a(b+V)})$ describes kinetics of (in)activation of the currents. The bifurcation parameter V_{K2}^{shift} is a deviation from $V_{1/2} = 0.018$ V corresponding to the half-activated potassium channel at $f = 1/2$. Dynamically, variations of V_{K2}^{shift} translate the *slow nullcline* $\dot{m}_{K2} = 0$ in the V direction, thereby altering the activation of I_{K2} . In this study, V_{K2}^{shift} varies within $[-0.026, 0.0018]$ V; these upper and lower values correspond to the hyperpolarized quiescent and tonic spiking states of the neuron, respectively. In between, the model exhibits multiple transformations of the bursting activity.

Because of the disparity of the time constants of the phase variables, the fast-slow system paradigm is applicable to system (1): Its first two equations form a fast subsystem, while the last equation is the slow one. The

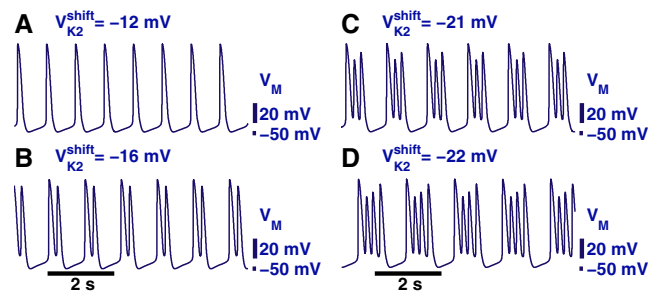


FIG. 1 (color online). An incremental spike adding cascade develops as the activation kinetics of the slow potassium current is shifted towards more depolarized membrane potentials.

dynamics of such a system are known [10] to be determined by and centered around attracting pieces of the slow motion manifolds that constitute a skeleton of activity patterns. These manifolds are formed by the limit sets, such as equilibria and limit cycles, of the fast subsystem where the slow variable becomes a parameter in the singular limit. A typical Hodgkin-Huxley model possesses a pair of such manifolds [11]: quiescent and tonic spiking, denoted by M_{eq} and M_{lc} , correspondingly. A solution of (1) that repeatedly switches between the low, hyperpolarized branch of M_{eq} and the spiking manifold M_{lc} represents a bursting activity in the model. In this Letter and our previous works [5–7], we reveal these manifolds in the full model (1) by employing the parameter continuation approach without the preceding slow-fast decomposition. This is the novelty of our approach based on the parameter dependence of solutions of the initial value problem. Observe first that, by construction, the equilibrium state of the full system is that of its fast subsystem. In the phase space of (1), it is the intersection point of the 1D quiescent manifold M_{eq} with the 2D slow nullcline $\dot{m}_{K2} = 0$, as shown in Figs. 2(a₁)–(c₁). The position of the latter depends on V_{K2}^{shift} . Hence, as V_{K2}^{shift} is varied, the equilibrium state of (1) and, therefore, the slow nullcline move (vertically) along, thereby tracing the desired manifold M_{eq} . Note that the V_{K2}^{shift} -parameter continuation leaves M_{eq} intact. This approach is especially applicable to multiple time scales systems where a similar continuation technique reveals the manifolds.

Whenever the spiking manifold M_{lc} is transient for the solutions of (1), such as the ones winding around it in Figs. 2 and 4, the model exhibits bursting. Otherwise, (1) has a spiking periodic orbit that has emerged on M_{lc} through the saddle-node bifurcation, thereby terminating the bursting activity [5,8], or both regimes may coexist as in Refs. [6,7]. In our earlier works, we developed the concept of the averaged nullclines specifically to locate and study local bifurcations of such spiking periodic orbits. Loosely speaking, one shall exist if the slow nullcline $\dot{m}_{K2} = 0$ cuts across the spiking manifold M_{lc} . Its position on M_{lc} is determined by that of the average slow nullcline, which, in turn, is determined by the bifurcation parameter V_{K2}^{shift} . Therefore, in response to a change in the value of V_{K2}^{shift} , the periodic orbit slides along the manifold M_{lc} . The parameter continuation of periodic orbit branches is a reliable numerical routine based on the collocation method or the boundary value problem, which are implemented in software packages such as CONTENT [12] used in this study. Thus, by following the orbit that represents the tonic spiking, we can trace down the whole spiking manifold and determine both its attracting and unstable segments. A partial segment of the manifold corresponding to V_{K2}^{shift} increasing from -0.026 mV (left end) through 0.0018 V, where M_{lc} wraps around M_{eq} , is shown in Figs. 2 and 4. The number of complete revolutions of the solution of (1) around M_{lc} is that of spikes per burst. We use this winding

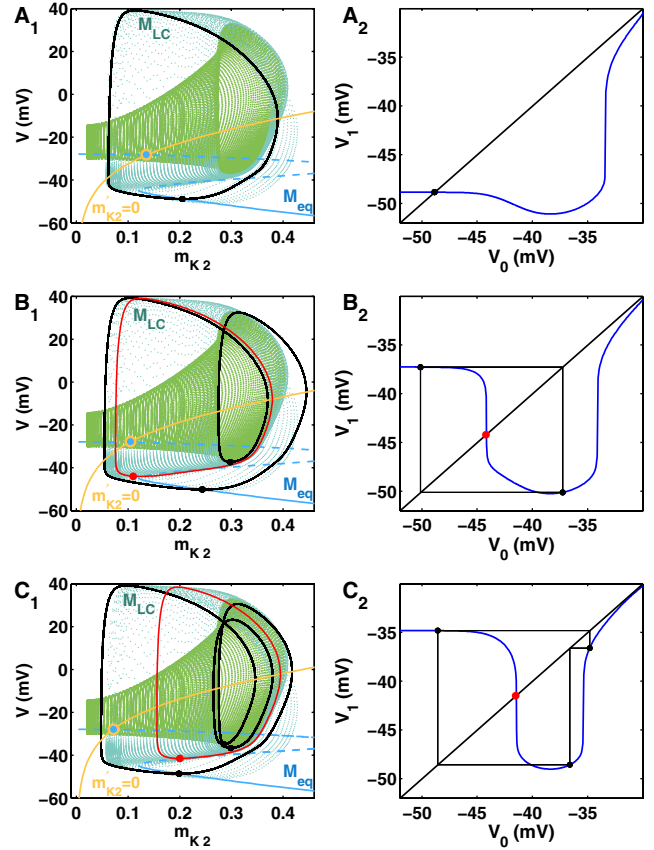


FIG. 2 (color online). Phase portraits (left column) and Poincaré mappings (right column) corresponding to the waveforms in Figs. 1(a)–1(c) for $V_{K2}^{shift} = -0.012$, -0.016 , and -0.021 V, respectively. (a) Unique minimum on the spiking orbit of (1) is the stable fixed point of the Poincaré mapping. In (b₂) and (c₂), this fixed point, now unstable (red dot), sets the threshold between the quiescent and spiking sections of the mapping graph. (b) Two V minima of the bursting orbit correspond to the period-2 attractor of the mapping. The two points of the latter are separated by the threshold, so that the left one represents the minimum at the quiescent phase and the one to the right corresponds to the minimum separating two spikes in the burst trace. (c) Three V minima of the bursting orbit compose the period-3 attractor of the mapping, consisting of one point corresponding to the quiescent phase while two points separate three spikes within the burst.

number to classify the bursting activity. The evolution of the bursting attractor corresponding to the waveforms in Fig. 1 is shown in the left column in Fig. 2. One can notice that its transformations occur on the aforementioned spiking manifold M_{lc} . To determine what makes the bursting attractor change its shape and stability, we construct numerically a V_{K2}^{shift} -parameter family of 1D Poincaré mappings taking an interval of membrane potentials onto itself. This interval is comprised of the minimal values, denoted by (V_0), of the membrane potential on the found periodic orbits foliating densely the spiking manifold M_{lc} . Then, for some V_{K2}^{shift} in question, we integrate numerically the outgoing solution of (1) starting from the initial conditions

corresponding to each (V_0) to find the consecutive minimum (V_1) in the voltage time series. All found pairs (V_0, V_1) constitute the graph of the Poincaré mapping for given V_{K2}^{shift} . Such a mapping, shown in Fig. 2(a₂) at $V_{K2}^{\text{shift}} = -0.012$ V, corresponds to the trace in Fig. 1(a). Its fixed point is a single V minimum on the periodic orbit in Fig. 2(a₁). The stability of the orbit follows from the fact that the fixed point resides on the flat quiescent section of the mapping graph that is constituted by the stable equilibria on the hyperpolarized branch of M_{eq} . Decreasing V_{K2}^{shift} below -0.0149 V results in (1) generating bursts with two spikes [Fig. 1(b)]. The mapping shows that the transition from tonic spiking into bursting occurs through the flip bifurcation, giving rise to a new period-2 bursting attractor. Further decreasing V_{K2}^{shift} below -0.0200812 V elevates the slow nullcline $\dot{m}_{K2} = 0$, thereby slowing down the m_{K2} component of the bursting orbit of (1) on M_{eq} so that the neuron starts to generate bursts with three spikes (Figs. 1 and 2). In the mapping, this is accompanied by the quiescent section of the mapping graph lifting up, so that the iterate of the bursting orbit, which follows its quiescent phase, is brought up higher into the spiking section of the mapping with more depolarized potentials. This increases the number of the points comprising the bursting orbit of the mapping and, correspondingly, makes the solution of (1) linger longer around the manifold M_{lc} and, hence, generate more spikes within the burst.

The whole spike adding sequence is documented in the bifurcation diagram in Fig. 3. It yields the evolution of the bursting orbits of the mappings and, therefore, of the V minima of the bursting orbits of model (1) as V_{K2}^{shift} is

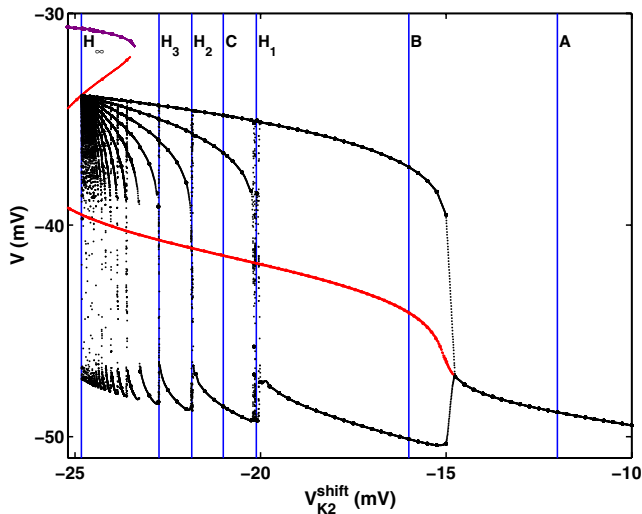


FIG. 3 (color online). Bifurcation diagram: stable and unstable orbits of the Poincaré mapping are shown in black/purple and red, respectively. The middle (red) branch of the diagram is the threshold between quiescent and spiking phases of the bursting. The fold point corresponds to the saddle-node bifurcation of fixed points of the Poincaré mapping. Parameter values labeled (a)–(c) are used in Figs. 1 and 2. Lines with H's mark homoclinic bifurcations and spike adding transitions.

varied. In Fig. 3, the number of the intersections of the vertical lines labeled by (a)–(c) yields the spike number per burst for the parameter values corresponding to Figs. 1 and 2. The diagram reveals also that spike adding transitions occur within narrow parameter windows where the system shows chaotic (or long transient) regimes (Fig. 4).

Chaos observed at a spike adding transition is due to the emerging homoclinics to the repelling (threshold) fixed point in the family of these noninvertible Poincaré mappings. Since its multiplier is negative, in the phase space of model (1) the image of the point is a saddle periodic orbit with 2D stable and unstable manifolds homeomorphic to a Möbius band [8]. A first boundary of the transition window corresponds to the occurrence of a primary homoclinic orbit induced through the initial tangency of these manifolds [13]. Inside the window, the tangles of the manifolds crossing transversally produce countably many Poincaré homoclinic and saddle periodic orbits. As a result, the system can generate burst trains with unpredictably alternating spike numbers. Such a situation is depicted in the transition window around the parameter cut H_1 , where the neuron model exhibits bursts with two, three, and four spikes. Figure 5 gives the distribution of the number of spikes per burst as the V_{K2}^{shift} is varied within this window.

Detection of homoclinics of a saddle periodic orbit in the phase space of a model is the state of the art. We use the Poincaré mapping technique to find the homoclinic orbits in the phase space of the interneuron model (1) and the corresponding parameter values indeed by following the forward iterates of the *critical* point on the graph of the corresponding mapping. The homoclinic tangency occurs when a finite sequence of the forward iterates of the critical point terminates at the repelling fixed point. Figure 4(d₂) shows a homoclinic orbit and chaos caused by it at the transition window between the robust bursts with 4–5 spikes. Overall, we detected the first 17 such primary homoclinic bifurcations (Fig. 6) which cause the spike adding transitions. The transitions occur more often as V_{K2}^{shift} decreases

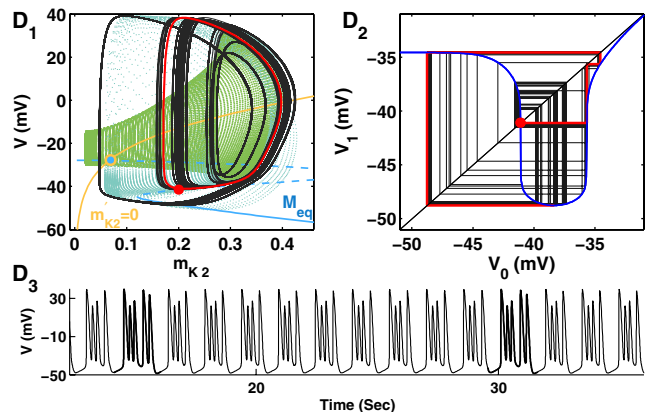


FIG. 4 (color online). Chaos in (1) and the mapping at the transition from 4 to 5 intraspikes per burst at $V_{K2}^{\text{shift}} = -0.02185302734375$ V. Shown in red are the saddle periodic orbit and the primary homoclinics to the threshold fixed point.

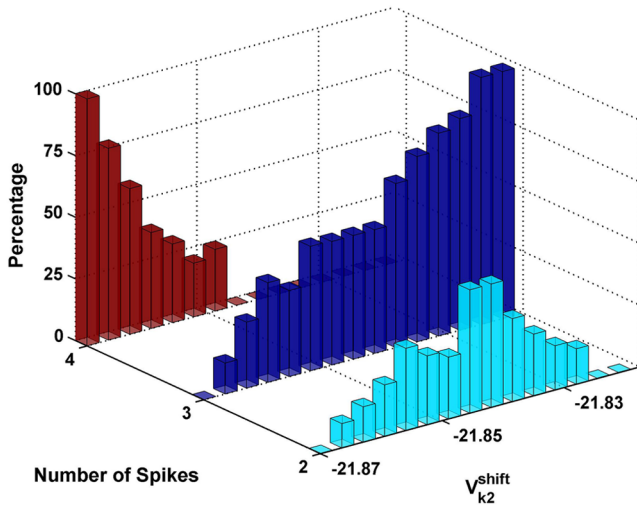


FIG. 5 (color online). Distribution of the number of spikes per burst through the transition window around $V_{K2}^{\text{shift}} = -0.02185$ V.

towards -0.024828 V, which corresponds to an arbitrarily long homoclinic orbit (Fig. 6).

In conclusion, we discuss the details of the forthcoming termination of the bursting activity in the interneuron model. The use of the mappings makes the interpretation of the scenario proposed in Ref. [6] particularly clear. The diagram in Fig. 3 shows the fold point corresponding to a saddle-node bifurcation at $V_{K2}^{\text{shift}} = -0.0265$ V. To its left, the mapping possesses a pair of new fixed points. The stable one (its branch shown in purple) is the only V minimum of the spiking periodic orbit that coexists now with the bursting attractor. The basins of both attractors are separated by the new unstable fixed point (upper red branch). A further decrease of V_{K2}^{shift} ceases the bistability, when the basin of the bursting attractor collides with the unstable point at $V_{K2}^{\text{shift}} = -0.024828$. The bursting's basin

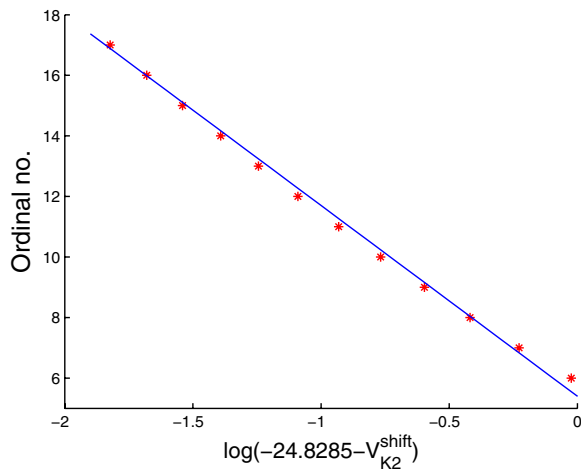


FIG. 6 (color online). Logarithmic fit of the sequence of the primary homoclinic bifurcation values accumulating to $V_{K2}^{\text{shift}} = -0.024828$ V, plotted vs the ordinal number of the homoclinic orbits.

becomes fractal for smaller values of the parameter, so that the bursting attractor is endowed with the Cantor set structure. The real cause of this crisis is the occurrence of a primary homoclinic of the new fixed point [13] that, in turn, establishes a heteroclinic connection between both unstable ones. After that, the system demonstrates transitive bursting for an indefinite time, prior to switching into the dominating tonic spiking regime.

We thank the anonymous reviewers for the helpful comments. This work was supported by NIH Grant No. NS-043098, the GSU Brains and Behavior program, and RFFI Grant No. 050100558.

*Electronic address: ashilnikov@gsu.edu

- [1] G. S. Cymbalyuk, Q. Gaudry, M. A. Masino, and R. L. Calabrese, *J. Neurosci.* **22**, 10580 (2002); S. Rinaldi and S. Muratori, *Ecol. Model.* **61**, 287 (1992); D. J. DeShazer, J. Garcia-Ojalvo, and R. Roy, *Phys. Rev. E* **67**, 036602 (2003).
- [2] M. Levi, *SIAM J. Appl. Math.* **50**, 943 (1990); Y.L. Maistrenko, V.L. Maistrenko, and S.I. Vikul, *Chaos Solitons Fractals* **9**, 67 (1998); V.S. Piassi, A. Tufaile, and J.C. Sartorelli, *Chaos* **14**, 477 (2004).
- [3] E. Mosekilde, B. Lading, S. Yanchuk, and Yu. Maistrenko, *BioSystems* **63**, 3 (2001); H. Gu, M. Yang, L. Li, Z. Liu, and W. Ren, *Phys. Lett. A* **319**, 89 (2003); A.L. Shilnikov and N.F. Rulkov, *Int. J. Bifurcation Chaos Appl. Sci. Eng.* **13**, 3325 (2003).
- [4] T.R. Chay, *Physica (Amsterdam)* **16D**, 233 (1985); A.V. Holden and Y.S. Fan, *Chaos Solitons Fractals* **2**, 221 (1992); B. Deng, *J. Math. Biol.* **38**, 21 (1999); V. Belykh, I. Belykh, E. Mosekilde, and M. Colding-Joergensen, *Eur. Phys. J. E* **3**, 205 (2000); A.L. Shilnikov and N.F. Rulkov, *Phys. Lett. A* **328**, 177 (2004); G.S. Medvedev, *Physica (Amsterdam)* **202D**, 37 (2005).
- [5] A. Shilnikov and G. Cymbalyuk, *Phys. Rev. Lett.* **94**, 048101 (2005).
- [6] A. Shilnikov, R.L. Calabrese, and G. Cymbalyuk, *Phys. Rev. E* **71**, 056214 (2005); *Neurocomputing* **65–66**, 869 (2005).
- [7] G. S. Cymbalyuk and A. L. Shilnikov, *J. Comput. Neurosci.* **18**, 255 (2005); *Reg. Chaotic Dyn.* **9**, 281 (2004).
- [8] L. P. Shilnikov, A. L. Shilnikov, D. V. Turaev, and L. O. Chua, *Methods of Qualitative Theory in Nonlinear Dynamics* (World Scientific, Singapore, 1998), Vol. I; *Methods Qualitative Theory in Nonlinear Dynamics* (World Scientific, Singapore, 2001), Vol. II; A. Shilnikov, L. P. Shilnikov, and D. Turaev, *Moscow Math. J.* **5**, 205 (2005).
- [9] G. S. Cymbalyuk and R. L. Calabrese, *Neurocomputing* **38–40**, 159 (2001).
- [10] A. N. Tikhonov, *Mat. Sb.* **31**, 575 (1952); N. Fenichel, *J. Diff. Equ.* **31**, 53 (1979).
- [11] J. Rinzel and B. Ermentrout, in *Methods in Neuronal Modelling: From Synapses to Networks*, edited by C. Koch and I. Segev (MIT, Cambridge, MA, 1989).
- [12] <ftp://ftp.cwi.nl/pub/CONTENT>.
- [13] N. K. Gavrilov and L. P. Shilnikov, *Math. USSR Sb.* **19**, 139 (1973).